Correspondence to:

K. Golubenko,
kseniia.golubenko@oulu.fi

Full Modeling and Practical Parameterization of Cosmogenic [10]Be Transport for Cosmic-Ray Studies: SOCOL-AERv2-BE Model

K. Golubenko[1] , **E. Rozanov[2,3]** , **G. Kovaltsov[4]**, **M. Baroni[5]** , **T. Sukhodolov[2]**, and **I. Usoskin[1]**

[1]Space Physics and Astronomy Research Unit and Sodankylä Geophysical Observatory, University of Oulu, Oulu, Finland, [2]Physikalisch-Meteorologisches Observatorium Davos and World Radiation Center, Davos Dorf, Switzerland, [3]Ozone Layer and Upper Atmosphere Research Laboratory, St. Petersburg State University, Saint Petersburg, Russia, [4]Ioffe Physical-Technical Institute, Saint Petersburg, Russia, [5]Aix Marseille University, CNRS, IRD, INRAE, CEREGE, Aix-en-Provence, France

Abstract A new full model of the atmospheric transport of cosmogenic [10]Be is presented based on the specialized SOCOL-AERv2-BE chemistry-climate model coupled with the CRAC:10Be isotope production model. The model includes all the relevant atmospheric processes and allows computing the isotope concentration at any given location and time. The full model is directly compared with [10]Be isotope measurements in five Antarctic and Greenland ice cores for the period 1980–2007. The model reasonably well reproduces the average concentration and solar-cycle dependency or the lack of it for most observational sites but does not perfectly catch the interannual variability at sites with complex orography likely due to the coarse model grid. This implies that the model correctly reproduces the large-scale atmospheric dynamics but effectively averages out synoptic-scale variability. It is found that the dominant source of [10]Be is located in the middle stratosphere (25–40 km), in the tropical (<30° latitudes) and polar (>60°) regions, as produced by galactic cosmic rays and solar energetic particles, respectively. It is shown that >60% (90%) of [10]Be produced in the atmosphere reaches the Earth's surface within one (two) years, respectively. For practical purposes, a simple parameterization of the full-model results is presented which agrees with the full model within 20% in polar regions. This parameterization allows one to make a quick estimate of near-ground [10]Be concentrations based only on production rates without heavy calculations. This practical approach can be applied to studies of solar and geomagnetic variability using cosmogenic isotopes.

1. Introduction

Cosmogenic isotopes (e.g., [10]Be, [7]Be, ^{14}C) are continuously produced in the Earth's atmosphere by galactic cosmic rays (GCRs) and sporadically by solar energetic particles (SEPs—see, e.g., reviews by Beer et al., 2012; Miyake et al., 2019; Usoskin, 2023). Solar activity modulates GCR fluxes leading to the ≈11-year solar cycle in the cosmogenic-isotope production rates. Due to the geomagnetic shielding, the isotope production has also a clear geographical pattern being the strongest in polar regions where the Earth's magnetic field is vertical and does not prevent the energetic particles from penetrating into the atmosphere, and weaker in the tropics (e.g., Lal & Suess, 1968; Usoskin et al., 2008). One of the most important proxies for solar-variability studies is cosmogenic isotope [10]Be measured in polar ice. Before reaching the surface, [10]Be can spend few years in the atmosphere (Delaygue et al., 2015) after its production. Accordingly, [10]Be atoms deposited in the polar ice are not necessarily produced locally but may be transported from farther regions. Thus, the measured [10]Be concentrations in polar ice cores are defined by not only the production rate but also by the atmospheric circulation and can be different in the northern and southern hemispheres (e.g., Butchart, 2014; Heikkilä et al., 2009). The latter is crucially important to correctly apply the isotope data to study cosmic-ray variability in the past. The origin of [10]Be deposited at a given location needs to be accurately modeled as the atmospheric state and dynamics introduce an important uncertainty of solar-activity reconstructions in the past (e.g., Delaygue & Bard, 2011).

Earlier studies of [10]Be measurements in ice cores (Dibb et al., 1994; Mazaud et al., 1994) considered the importance of atmospheric transport processes but were based on crude approximations, neglecting many important features. For example, the isotope deposition in polar ice was assumed to reflect only the regional polar production of [10]Be or, on the contrary, [10]Be was assumed to be well-mixed representing the global production, while in reality it is strongly affected by precipitation, resulting in large regional differences in deposition fluxes.

In an attempt to parameterize this, Bard et al. (1997) proposed the so-called Polar Enhancement Coefficient (PEC) relating the Antarctic ^{10}Be concentrations with the globally mixed ^{14}C data. McCracken (2004) proposed another purely empirical approach linking the ^{10}Be production to its deposition by using various ad-hoc assumptions of atmospheric mixing and their latitude dependence. We note that such simplistic approaches are still in use (e.g., Adolphi et al., 2023) because of the lack of a readily applicable full model.

Field et al. (2006) developed the first beryllium transport model based on the Goddard Institute for Space Studies general circulation model (GISS GCM ModelE). Such models are usually compared with in-air measurements of the short-living (half-life of about 53 days) isotope of beryllium ^{7}Be since these measurements are relatively easy to do and are routinely performed by the Comprehensive Nuclear-Test-Ban Treaty Organization (CTBTO— https://www.ctbto.org) at numerous locations around the globe (e.g., Leppänen et al., 2010). The GISS model was successfully tested by reproducing the measured ^{7}Be concentrations in the near-ground air (Usoskin, Field, et al., 2009) but had difficulties in ascribing specific causes of the ^{10}Be variability in ice core records, particularly in distinguishing between climate-related and solar-related changes. Unfortunately, that model was not developed further and cannot be readily used now.

This approach was developed further by Ulla Heikkilä and co-workers in a series of papers (e.g., Heikkilä, Beer, et al., 2013; Heikkilä et al., 2009) who presented realistic full transport modeling of beryllium isotopes in the atmosphere, based on the ECHAM5-HAM atmospheric model, and concluded that the stratospheric component is dominant (70%) in ^{10}Be polar deposition. In the tropospheric part (30%), half of the ^{10}Be in polar ice cores was found to originate from the subtropics and another half from polar latitudes, while the contribution from ^{10}Be produced in the tropics or the opposite hemisphere is negligible. Since the full modeling is time-consuming, especially when applied to different climatic conditions of the past requiring long spin-ups, a simple parameterization of the model ^{10}Be output was made in the form of the weights of six production boxes in each hemisphere (Heikkilä, Beer, et al., 2013). This parameterization has been widely used to study beryllium data in polar ice (e.g., Usoskin et al., 2016; Wu et al., 2018), but it was defined only for GCR and cannot be readily applied to SEP-related production of the isotope.

The previous studies, discussed above, utilized the isotope production model introduced by Masarik and Beer (1999), which is presently outdated, and even more importantly, is based on prescribed spectra of GCR and cannot be applied to the cosmogenic isotopes produced by SEPs. As shown by Golubenko et al. (2022), a recent ^{10}Be-isotope yield function based on the CRAC (Cosmic-Ray Atmospheric Cascade) model (Poluianov et al., 2016) is more precise to model the isotope's atmospheric production and can be directly used also for SEPs. This justifies the need for an update of the atmospheric ^{10}Be transport modeling, particularly for studies of the recently discovered extreme SEP events (Cliver et al., 2022; Miyake et al., 2012; Usoskin et al., 2013).

Several modeling efforts to model beryllium transport in the atmosphere have been undertaken recently. Spiegl et al. (2022) used the ECHAM/MESSy Atmospheric Chemistry (EMAC) model for atmospheric transport and Warning System for Aviation Exposure to SEP (WASAVIES) for the isotope production. That model focuses on the SEP production and does not consider the continuous ^{10}Be production by GCRs. Another approach (Zheng et al., 2023, 2024) was based on ECHAM6.3-HAM2.3 and GEOS-Chem models and was focused on the GCR source and a case study of the AD 774 extreme SEP event. A realistic modeling of the transport and deposition of ^{10}Be produced by SEPs in the atmosphere was performed by Sukhodolov et al. (2017) using the chemistry-climate mode (CCM) SOCOL (a modeling tool for studies of SOlar Climate Ozone Links). This model combines both the GCR and the SEP sources and reproduces well the observed SEP-induced peaks, showing the consistency between the modeled and measured ^{10}Be SEP-signal within 10–20%. However, that model version used a simplified treatment of deposition processes, which complicated the seasonal and regional attribution of deposition signals. Moreover, the modeling by Sukhodolov et al. (2017) was performed for a specific period around AD775 and cannot be readily applied to other conditions. Although these models reasonably well reproduce the observed beryllium data for specific conditions studied, they can hardly be applied to other conditions (e.g., geomagnetic) without a full re-modeling.

Here, we further develop the direct model of atmospheric cosmogenic-isotope transport by updating a new version of SOCOL, viz. SOCOL-AERv2-BE (Golubenko, Rozanov, Kovaltsov, et al., 2021), which includes an explicit treatment of removal processes in the troposphere (Feinberg et al., 2019), combined with the latest updated production estimates for GCR (Usoskin et al., 2017) and SEP (Koldobskiy et al., 2021). We aim to synthesize the focuses and advances of previous studies in one modeling set-up, by looking at both galactic and

solar ^{10}Be sources, dividing their production into multiple source regions, and independently modeling the atmospheric transport and deposition of the resulting tracers. Such a modeling set-up allows us to track how much each of the individual source regions in the atmosphere contributes to the ice core locations and how different it is for CGR and SEP. We base our study on the recent 1980–2007 period, due to the availability of reliable data for atmospheric dynamics and ice core measurements for validation. Simulation results are then used to construct a new simple parameterization that can be widely used to relate the production of ^{10}Be to its deposition. As the main result of this work, we also provide a handy parameterization of the full model that can be used for direct quick assessments of ^{10}Be concentrations in polar air and thus cosmic-ray variability, without a full re-modeling.

2. Model Description

2.1. Production of ^{10}Be: CRAC Model

Production of ^{10}Be was computed using the CRAC (Cosmic-Ray Atmospheric Cascade) model (Poluianov et al., 2016) which is the most recent, precise and validated dedicated model of cosmogenic isotope production. This model simulates, using the GEANT4 Monte Carlo simulation tool (Agostinelli et al., 2003), the full nucleonic-muon-electromagnetic cascade induced by primary cosmic-ray particles in the atmosphere. Originally developed by Usoskin and Kovaltsov (2008) and Kovaltsov and Usoskin (2010), the CRAC model was subsequently updated and improved by Poluianov et al. (2016). The model provides a set of precisely computed yield functions for the production of cosmogenic isotopes by different primary particle types (viz. protons and α-particles, the latter effectively representing all heavier species), energy and atmospheric depths. It has been directly validated against the data of ^{7}Be measurements in near-ground air (Golubenko, Rozanov, Kovaltsov, et al., 2021). The isotope's production rate q can be computed for a given location via the geomagnetic rigidity cutoff P_c (e.g., Cooke et al., 1991; Herbst et al., 2013), atmospheric height h (via the residual atmospheric depth or barometric pressure) and time (via the time-variable energy spectrum):

$$q(h, P_c, t) = \sum_m \int_{E_{c,m}}^{\infty} J_m(E, t) \cdot Y_m(E, h) \cdot dE, \qquad (1)$$

where $J_m(E,t)$ is the intensity of incident cosmic ray particles of the mth type (characterized by the charge Z_m and atomic mass A_m numbers), $Y_m(E, h)$ is the isotope yield function, E is the kinetic energy per nucleon of the incident particle, h is the atmospheric depth; $E_{c,m}$ defined as

$$E_{c,m} = \sqrt{\left(\frac{P_c \cdot Z_m}{A_m}\right)^2 + E_0^2} - E_0 \qquad (2)$$

is the energy corresponding to the local geomagnetic cutoff rigidity P_c for a particle, where $E_0 = 938$ MeV is the proton's rest mass. Summation in Equation 1 is over different types of primary particles.

Energy spectra of GCR were computed in the framework of the force-field approximation (Caballero-Lopez et al., 2004; Usoskin et al., 2005, 2011) using the modulation potential ϕ calculated from the data of the worldwide neutron-monitor network (Usoskin et al., 2017; Väisänen et al., 2023), and the local interstellar spectrum of GCR parameterized by Vos and Potgieter (2015). As the energy spectrum of SEPs, we considered a hard spectrum of the second strongest and one of the best studied SEP events of 20-Jan-2005 (GLE #69—see http://gle.oulu.fi) computed by Koldobskiy et al. (2021).

2.2. Beryllium Transport: SOCOL Model

The computed isotope production rates were further used as an input for the CCM SOCOL-AERv2-BE, which is based on the SOCOL-AERv2 model (Feinberg et al., 2019) extended with the beryllium module (Golubenko, Rozanov, Kovaltsov, et al., 2021). This model consists of the general circulation model MA-ECHAM5 (Hommel et al., 2011) and the atmospheric chemistry module MEZON (Model for investigating ozone trends—Egorova et al., 2003), interacting with each other every two modeling hours. In this study, the MA-ECHAM5 dynamics was nudged toward the meteorological data from ECMWF (European Center for Medium-Range Weather Forecasts) atmospheric reanalysis data of the global climate ERA-Interim

Table 1
Production Zones of ^{10}Be Model Tracers Considered Here

Zone	Code		Notation	Range	Approx. location
Latitude	i =	1	S1	60°–90°S	South polar
		2	S2	30°–60°S	South mid-lat
		3	S3	0°–30°S	South tropics
		4	N3	0°–30°N	North tropics
		5	N2	30°S–60°N	North mid-lat
		6	N1	60°S–90°N	North polar
Altitude	j =	1	Tr	0–10 km	Troposphere[a]
		2	St1	10–35 km	Stratosphere[a]
		3	St2	35–55 km	Upper stratosphere
		4	Mez	55–80 km	Mesosphere
Longitude	k =	1	L1	0°–90°E	European sector
		2	L2	90°–180°E	Asian sector
		3	L3	180°–270°E	American sector
		4	L4	270°–360°E	Atlantic sector

[a]May differ from the realistic tropopause.

(eraiaT42L39) reanalyzes (Dee et al., 2011; Hersbach et al., 2020). The CCM SOCOL-AERv2-BE utilizes the Gaussian transform horizontal grid with the T42 triangular truncation (64 latitudes and 128 longitudes) splitting the model space into grid cells of about 2.8° × 2.8° size. The model's vertical-direction grid consists of 39 levels in the hybrid sigma–pressure coordinate system covering the altitudes ranging from the ground surface to about 80 km (0.01 hPa). The real orography is smoothed over the model grid cells (Stenke et al., 2013). Although the importance of volcanic events has been hypothesized for ^{10}Be signatures in ice cores (Baroni et al., 2019), the transport of ^{10}Be was modeled here as a gas, without taking into account its attachment to stratospheric aerosols and related gravitational sedimentation. This model update and the investigation of the volcanic contributions are planned for future study.

2.3. Model Experiment Set Up

Taking into account the typical age of stratospheric air, which is mostly defined by its slow meridional circulation (Butchart, 2014), we have performed a 6-year spin-up of the model for the period 1974–1980 to allow ^{10}Be to reach stable conditions in the entire atmosphere. After the spin-up period, we initiated a 28-year (1980–2007) run with a full nudging (a linear relaxation of thermodynamic parameters: temperature, divergence, and vorticity of the wind field) to the ERA-Interim reanalysis as described in Section 2.2. To analyze the transport and deposition of beryllium in more detail, we introduced, in addition to the general ^{10}Be tracer, 96 separate ^{10}Be tracers corresponding to the source regions where they have been produced by cosmic rays. The general tracer is identical to the sum of the 96 detailed tracers. The source regions and their notations are specified in Table 1 as six latitudinal zones (polar, mid-latitude and tropics for each hemisphere separately), four longitudinal sectors (European, Asian, American and Atlantic), and four altitude zones (troposphere, lower stratosphere, upper stratosphere and mesosphere). For instance, the N1L2St2 tracer corresponds to ^{10}Be produced in the northern polar region (N1), the Asian sector (L2) in the upper stratosphere (St2)—see Table 1 for details.

Model experiments were made for two distinct scenarios of ^{10}Be production, as described below. Each scenario was modeled in a dedicated run with all the 97 ^{10}Be tracers for each scenario separately.

Scenario 1 (*GCR*): continuous realistic production of ^{10}Be by GCRs whose variability was modeled as described in Section 2.1. Geomagnetic shielding was considered via the excentric-tilted-dipole approximation (Nevalainen et al., 2013) using the IGRF (International Geomagnetic Reference Field → Thébault et al. (2015)) data set.

Scenario 2 (*SEP*): Only production of ^{10}Be by SEPs is considered as quantified by GLE #69 (Koldobskiy et al., 2021) which originally took place on 20-Jan-2005 but was modeled here to take place during the day of 20-Jan-1980. After that day, no further production was considered, but beryllium was traced further.

3. Model Validation

3.1. Data Sets of ^{10}Be Measurements

To validate the model, we compared the simulated ^{10}Be near-surface concentrations with those measured in several ice cores, with the yearly sampling performed in both hemispheres for the period 1980–2007.

Since the ^{10}Be signal in an ice core can be affected not only by the production, viz. solar and geomagnetic modulation of cosmic rays but also by the atmospheric transport and deposition, data from multiple locations, preferably from the opposite polar regions are needed to exclude the regional climate influence. Here we use data from five high-latitude locations—two in Greenland and three in Antarctica (see Table 2 and Figure 1). For two Antarctic ice cores (Vostok and Dome C), ^{10}Be ice samples were prepared according to the

Table 2
List of Ice-Core Sites Used for the Present Study

Site	Region	Location, altitude	Source	Time interval
Neumayer	Antarctica	70°40S 8°16′W, 43 m	E11	1983–2007
Vostok	Antarctica	78°27′S 106°5′E, 3.5 km	B19	1980–2005
Dome C	Antarctica	75°05′S 123°7′E, 3.2 km	B19	1980–2005
DAS-2	Greenland	67°5′N 36°1′W, 2.9 km	Z20	1980–2003
NEEM	Greenland	77°27′N 51°4′W, 2.5 km	Z20	1980–2003

Note. The listed time intervals refer to the data used in this study, not to the total length of the data series. References are denoted as E11 (Elsässer et al., 2011), B19 (Baroni et al., 2019) and Z20 (Zheng et al., 2020).

procedure described by Baroni et al. (2019) and were measured using the French Accelerator Mass Spectrometer (AMS) national facility, ASTER (Arnold et al., 2010). For the Neumayer station, aerosol samples were continuously collected on (pre-cleaned) double cellulose filters over periods ranging from few days to several weeks (typically 14 days). ^{10}Be was extracted from filter aliquots for subsequent AMS analyses (Elsässer et al., 2011). For the Greenland stations, dating of the ice cores and derivation of annual accumulation rates of ^{10}Be followed a method by van Ommen and Morgan (2010) and the samples were prepared according to the procedure described in Pedro et al. (2012). ^{10}Be measurements were conducted at the ANTARES AMS facility, ANSTO, Australia (Simon et al., 2013).

3.2. Beryllium Transfer Function From the Atmosphere to the Snow

The model provides the concentration of ^{10}Be in the air, measured in atoms per cubic meter of air (at/m^3), whereas the ^{10}Be concentration in snow or ice samples is expressed in atoms per gram of ice. Consequently, a direct comparison between the ^{10}Be concentrations in the air and in the ice is not feasible unless we know the transfer function from the air to the surface.

It is known that ^{10}Be present in the air column doesn't necessarily settle immediately at the surface due to such factors as wind, atmospheric circulation, and the remobilization of snow layers. These complexities make it hardly possible to calculate the precise air-to-snow transfer function which may vary between different locations. To address this challenge, we employ an empirically determined adjustment coefficient to reduce the modeled beryllium concentration in surface air (given in at/m^3) to the measured concentration of ^{10}Be in ice (in at/g).

To establish this adjustment coefficient, we utilized both the ^{10}Be concentration data obtained from aerosol filters collected weekly in the atmosphere at Dome C in Antarctica in 2008 (Legrand, Preunkert, Wolff, et al., 2017), and ^{10}Be concentration data from a snow pit at Dome C (Baroni et al., 2019). The annual average ^{10}Be concentration in aerosol filters was found to be 2.6×10^4 at/m^3, while the ^{10}Be snow concentration in 2008 was 6.6×10^4 at/g. The ratio of the two values gives an estimate of the conversion factor of about 0.39 g/m^3. This conversion can be validated using another chemical component, such as sodium (Na$^+$), which serves as a proxy for sea-salt aerosols transported in the troposphere. It behaves similarly to ^{10}Be once it reaches the atmosphere above Dome C, as it is also attached to aerosols. The annual Na$^+$ concentration measured from aerosol filters over the period 2006–2015 at Dome C is 6.9 ± 1.1 ng/m^3 (Legrand, Preunkert, Weller, et al., 2017). This represents the Na$^+$ concentration in the atmosphere, while the Na$^+$ concentration in the Dome C snow pit
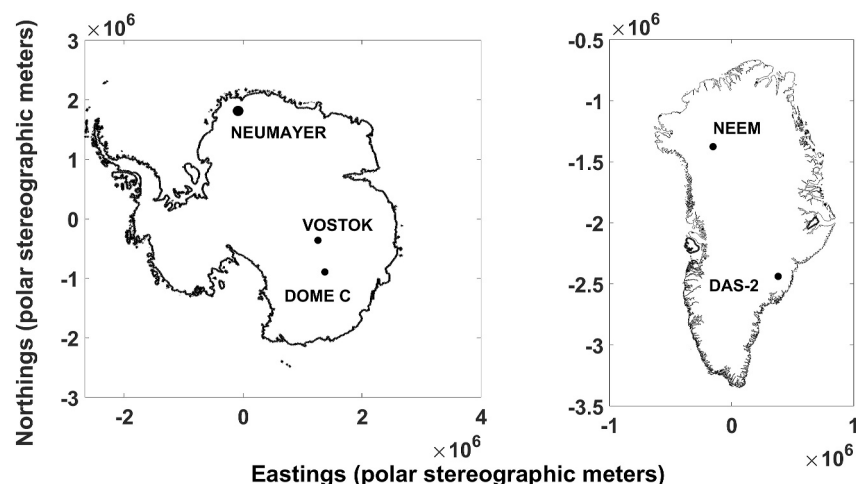

Figure 1. Location of ^{10}Be ice cores used in this study (see Table 2). Left- and right-hand-side panels are for Antarctica and Greenland, respectively.
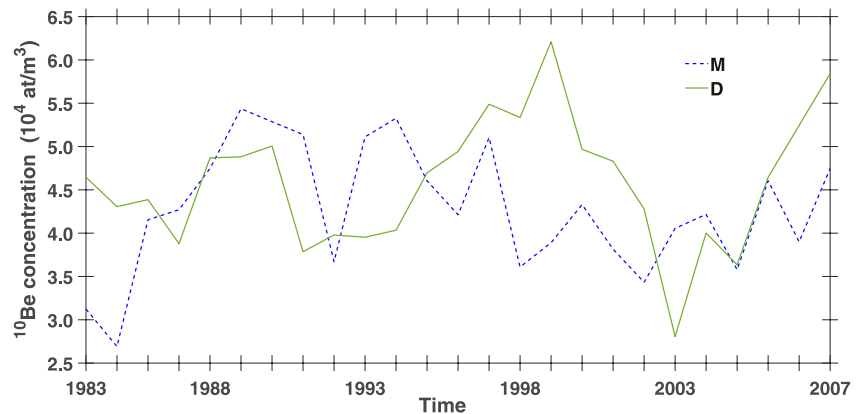
Figure 2. Time profiles of annual ^{10}Be in-air concentrations for the Neumayer site. Measured (D—data) and modeled (M—model) concentrations are depicted with green and blue dashed curves, respectively. Since the Neumayer station is located close to the boundary of the model's grid cells, the average value of concentration in these cells is shown for the model results.

(Baroni et al., 2019) from 2006 to 2012 (at the top of the snow pit) was 16 ng/g. The conversion factor for Na$^+$ is thus 0.43 g/m^3, which is similar to the value found for ^{10}Be.

Thus, for Dome C, we can approximate the transfer function of ^{10}Be from the atmosphere to the snow using a simple conversion factor of 0.39 g/m^3. However, this factor can be location-specific and ideally should be determined for each studied site individually, as the transfer function may differ between locations, particularly between coastal and continental regions in Antarctica and Greenland. However, the necessary data sets are not readily available for other sides. We are aware of this limitation and additional uncertainty, especially for the coastal DAS-2 site as discussed below in greater detail.

3.3. Comparison

In this Section, we compare the model's results with measurements of ^{10}Be in polar regions. Since the SEP contribution to the averaged production of ^{10}Be is negligible (<1%) compared to GCRs (Golubenko et al., 2022; Usoskin et al., 2020), we considered only the latter. First, we validated the model's output directly against ^{10}Be concentrations measured on air-borne aerosols using concentrations measured on aerosol filters at the Neumayer site for 1983–2007. The station is quite challenging to model due to its orographic and geographical peculiarities. Located on the Ekstrom ice shelf about 10 km inland from the ice edge, the station experiences strong winds and intensive aerosol scavenging year-round, with a low persistence of strong surface inversions and a relatively weak influence of inland air masses (Elsässer et al., 2011). The comparison between the annually averaged concentrations is shown in Figure 2. The mean measured concentration $(4.3 \pm 0.15) \cdot 10^4$ at/m^3 is well reproduced by the model $(4.58 \pm 0.15) \cdot 10^4$ at/m^3—the values agree within 7% and are statistically indistinguishable. However, the interannual variability is not precisely reproduced, likely because of the complex orography of the location which the model's grid cannot capture. The dominance of the regional climate in the beryllium concentrations at the Neumayer location can be seen in the absence of the 11-year cycle in the measured data that is correctly (no 11-year cycle) reproduced by the model, even though the solar cycle dominates the isotope's production. Additionally, there is no distinct seasonal cycle in ^{10}Be concentrations.

For the sake of comparability between results from the northern and southern hemispheres, we subsequently perform analyses only on ice-core stations (two stations per hemisphere), utilizing the concentration conversion coefficient from snow to air as empirically established for Dome C (Section 3.2). Figure 3 depicts the comparison between the measured and modeled annual concentrations of ^{10}Be in polar ice cores. To indicate the 11-year solar cycle in the isotope's production, the (inverted) annual Cosmic ray modulation potential (ϕ in MV) reconstructed from ground-based neutron-monitor data (https://cosmicrays.oulu.fi/phi/phi.html) are shown on the top panels.

First, we compared the annually averaged modeled and (converted as described in Section 3.2) measured concentrations. On the one hand, the agreement in the overall level of ^{10}Be concentration between the model output
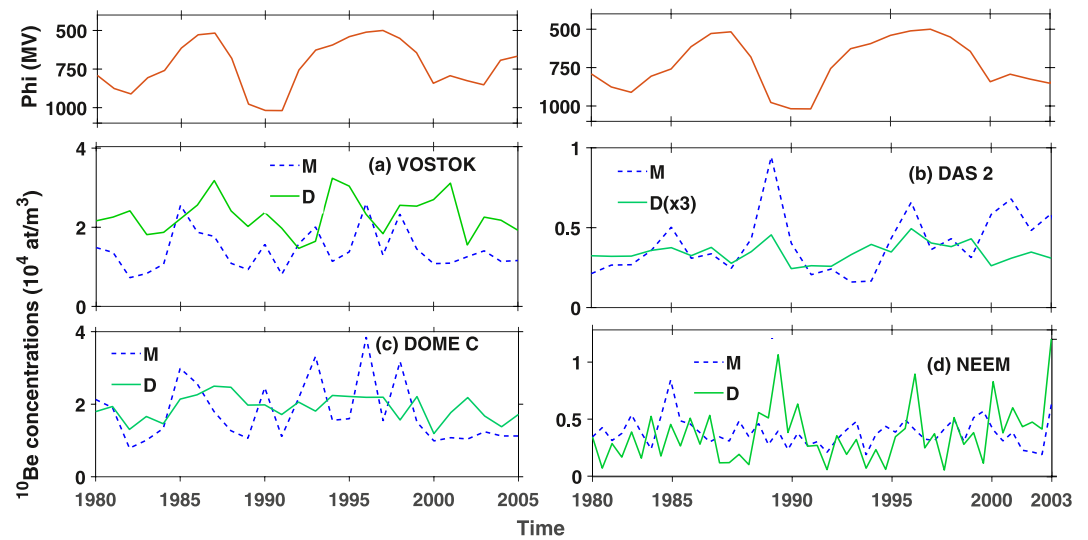
Figure 3. Time profiles of annual ^{10}Be concentrations (converted into the atmospheric concentration as discussed in Section 3.2) for the four sites used here (Table 2). Measured (D—data) and modeled (M—model) concentrations are depicted with solid green and blue dashed curves, respectively. For the modeled concentration for the Vostok site, we used the concentration of the closest model point. For the modeled concentration for DOME C, we used the average value of the two nearest model points. For the Greenland sites with complex orography, the zonal mean model concentrations were used. For DAS-2, it was scaled up by a factor of three. The inverted annual Cosmic ray modulation potential (ϕ in MV) reconstructed from ground-based neutron-monitor data (Usoskin et al., 2017) is shown as the red curve (top panel).

and the converted measured concentrations is accurate within a few per cent for Dome C (panel c) and NEEM (panel d) data sets suggesting that the model makes a good job computing the near-ground air concentrations of beryllium at these locations. It is important that the model computes the in-air beryllium concentrations directly without any ad-hoc adjustments/calibrations to the measured values and the conversion (Section 3.2) is purely empirical as based on the measured data only. On the other hand, the model underestimates the measured
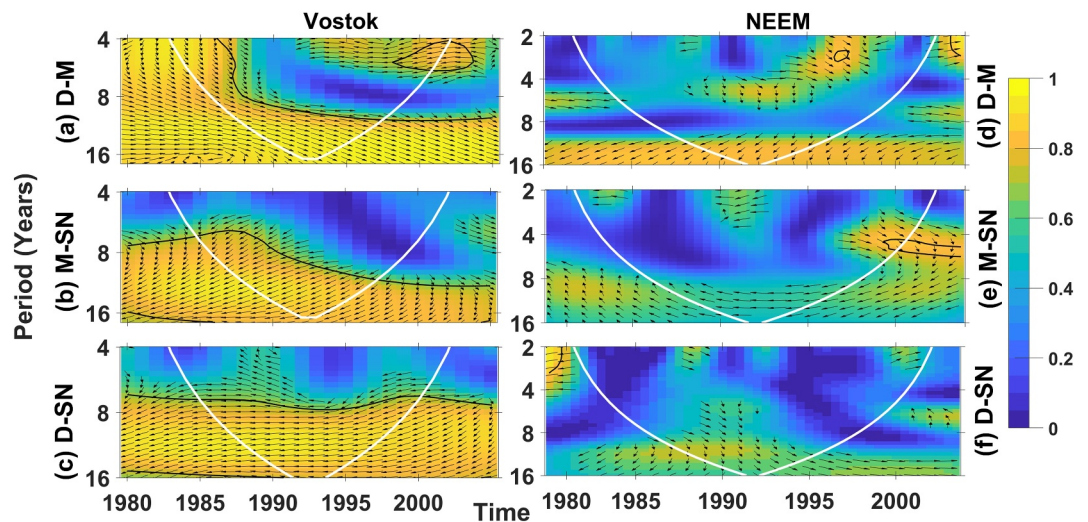
Figure 4. Wavelet coherence between sunspot number (SN), modeled (M) and measured (D) ^{10}Be activity for the Vostok (left-hand-side panels) and NEEM (right-hand-side panels) stations as indicated aside of each panel. The color scale represents the coherence level (from zero to unity via deep blue through yellow color), while the arrows denote the coherence phase (arrows pointing to the right/left denote in-phase/anti-phase relations, respectively). Thick black curves bound the 95% confidence levels against the AR1 red noise. The white curves bound the cone of influence within which the results are not trustable because of the edge effects.

Table 3
The Results of the Coherence Analysis Between Different Time Series at the Solar-Cycle Timescale for the Four Locations Studied Here (Table 2)

Data series	D-M	M-SN	D-SN
Vostok	Yes (1–2 years)	Yes (1–2 years)	Yes (0 years)
Dome C	Yes[a] (≈1 year)	ins (2–3 years)	Yes (0 years)
NEEM	ins (3–4 years)	ins (0 years)	ins (2–3 years)
DAS-2	ins (≈3 years)	ins (≤1 year)	ins (2–3 years)

Note. "D," "M" and "SN" denote the measured data, model results and the sunspot number, respectively. "yes" and "ins" stand for statistically significant ($p < 0.05$) and insignificant coherence, respectively, while the values in parentheses indicate the mean time shift between the series. [a]Before 1990.

(converted) concentrations by 35% for the Vostok site (panel a). This difference can be primarily due to the limited lateral resolution of the model (the grid size is ≈ 300 km in the meridional direction) and complex orography of the area (Stenke et al., 2013). The difference between the modeled and obtained from measurements concentrations is large, by a factor of three (the model overestimates the concentrations) for the DAS-2 site (panel b). This difference is too large to be ascribed to the local orography and is likely related to the incorrectness of the application of the in-ice-to-in-air conversion factor of 0.39 g/m^3, obtained for the Antarctic plateau (Legrand, Preunkert, Weller, et al., 2017), to the coastal Greenland site.

Next, we analyzed the interannual variability of the near-ground concentrations of ^{10}Be at different sites. Although the isotope's production is mostly governed by the GCR variability, viz. the solar cycle, which is intrinsically included in the isotope's production model, both the modeled and measured near-surface concentrations depict more variability (Figure 3) as caused by the regional circulation patterns. The solar cycle is relatively well visible in the Antarctic data but not observable in the Greenland data sets, where the regional climate is more variable and dominates the variability of the concentrations. A likely reason for the difference between the northern (no solar cycle) and southern (pronounced solar cycle) polar-region patterns is that planetary waves are stronger in the northern hemisphere than in the southern one and, as a consequence, concentrations are more influenced by the local air circulation there. The difference in the ^{10}Be deposition between the Southern and Northern hemispheres was also noted by Zheng et al. (2020). This pattern is generally consistent between the modeled and measured data sets, although the details may be different (Golubenko et al., 2022).

A visual inspection of overplotted curves may be imprecise. Here we also performed a wavelet-coherence analysis of the data series depicted in Figure 3. Wavelet coherence is an expansion of the cross-correlation analysis between two signals into the time-frequency-phase domain (e.g., Grinsted et al., 2004). The coherence takes the values between zero (no coherence) and unity (full coherence) as centered at a given time and frequency/period. In addition, the phase of the coherence is evaluated between zero (in-phase coherence) through 180° (anti-phase coherence). We used the Morlet-basis wavelet with the wavelet parameter $k = 3$ following the algorithm by Grinsted et al. (2004), which includes the estimation of the statistical significance against the autoregressive (red) noise AR1. Figure 4 shows the wavelet pairwise coherence between the ^{10}Be concentrations for two sites, Vostok and NEEM.

For the Vostok site, the coherence between modeled (M) and measured (D) data (Figure 4a) is highly significant at the timescale longer than 9 years, viz. the solar-cycle scale, throughout the entire interval and at a shorter timescale before 1986 and after 2000. The relative phasing between the two data series is slightly offset by about 1 year as seen in the arrows pointing at 30–45° down in Figure 4a. The agreement between the modeled (M) data and sunspot number (SN) data series (Figure 4b) is highly significant at the timescale longer than 8–10 years, with the beryllium concentration being in a general anti-phase relation with about a 1-year delay (arrows pointing left-down in Figure 4b) due to the atmospheric transport, as expected. The measured Vostok data (D) depict a highly significant coherence with the SN with an anti-phase relation (arrows pointing left in Figure 4c) which leaves no room for atmospheric transport. This discrepancy in about 1 year in synchronization of phasing between modeled and measured data sets can be due to insufficient dating accuracy of the measured data (Baroni et al., 2011).

The pairwise coherence for the NEEM Greenland site is poor for all combinations as seen in Figure 4 (Panels d–f) except for a few coherence spots. Interestingly, there is no statistically significant coherence between the modeled and measured concentrations even though the mean levels agree well (Figure 3d). Moreover, there is a phase shift corresponding to 3–4 years. This suggests that the very local transport/deposition patterns dominate the ^{10}Be concentrations at an interannual timescale in Central Greenland.

The results of the wavelet-coherence analysis for these and other data sets are summarized in Table 3. The statistically significant coherence at the solar-cycle timescale is observed only for the Antarctic sites—constantly for Vostok (Figures 4a–c) and intermittently for Dome C (not shown). The coherence is visible also for the Greenland sites, but it is insignificant implying that the regional climate signal dominates over the production there, at this timescale (cf., Usoskin, Horiuchi, et al., 2009).
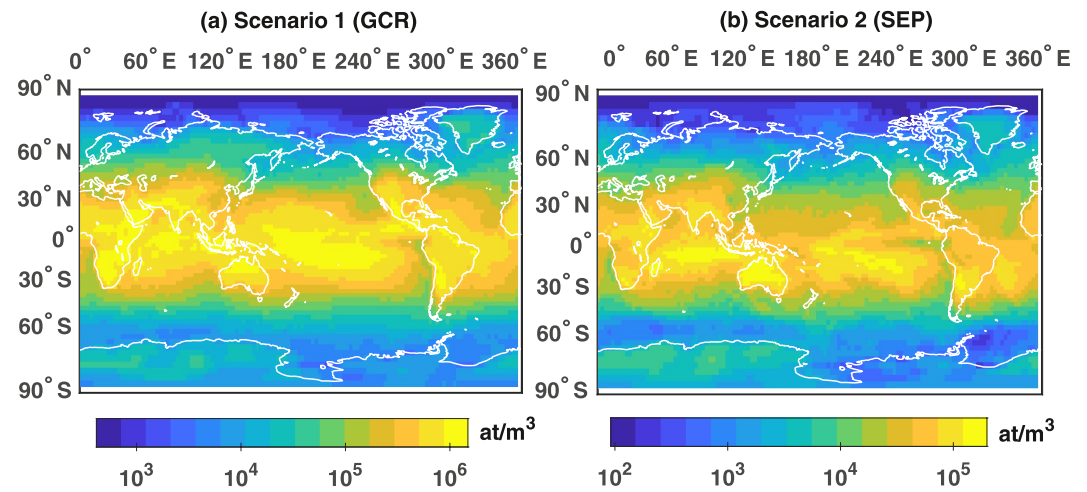
Figure 5. Geographical distribution of the ^{10}Be concentration (atoms/m^3) in the near-ground air according to the full model simulations for the two scenarios. Panel (a) concentration averaged throughout 1980–2007 for scenario 1 (GCRs, see Section 2.3). Panel (b) concentration averaged over one year after the modeled SEP event (20-Jan-1980 through 19-Jan-1981) for Scenario 2 (SEP, see Section 2.3).

Thus, while the detailed year-to-year variability of the ^{10}Be concentration is not precisely reproduced by the model for the four analyzed sites, the model correctly catches the overall pattern at the solar-cycle timescale, viz. whether the solar-cycle production (for Antarctic locations) or regional climate variability (for Greenland locations) dominates the beryllium concentration.

4. Results and Discussions

4.1. Geographical Distribution of ^{10}Be Concentrations

As an example of the model results, we show in Figure 5 the distribution of the ^{10}Be concentration in the near-ground air for the two scenarios described in Section 2.3: GCR and SEP. The concentrations are averaged over the entire period of 1980–2007 and one full year past the modeled event for the GCR and SEP scenarios, respectively. As seen, the highest ^{10}Be concentrations up to $7 \cdot 10^6$ at/m^3 are predicted in the tropics, over the Pacific, near-East
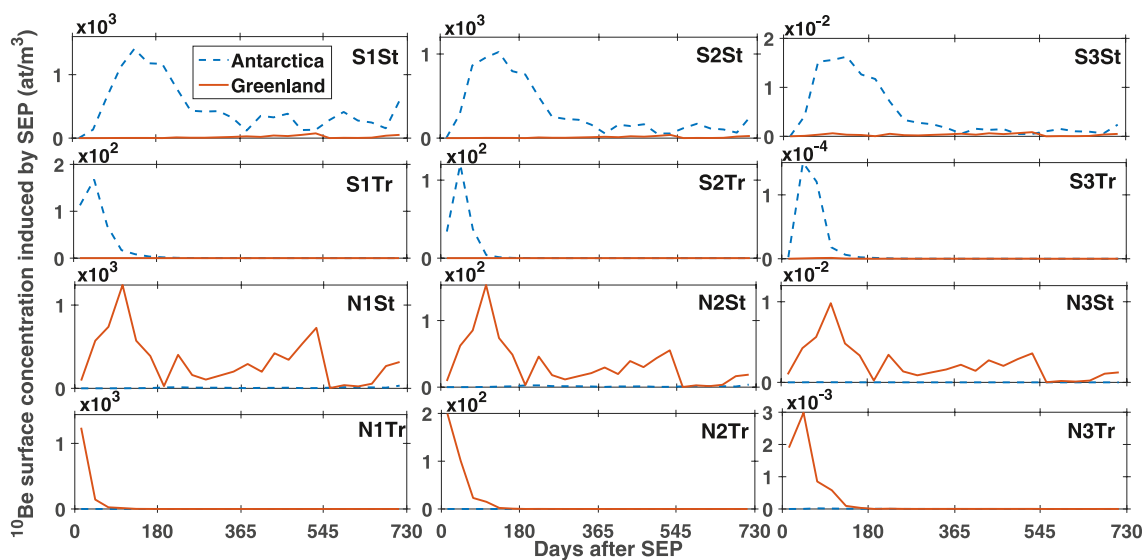

Figure 6. Zonal mean concentration of different ^{10}Be tracers in the near-ground air at Antarctica (blue curves) and Greenland (red curves), as a function of time past the modeled SEP event on day zero. Different panels represent different ^{10}Be tracers corresponding to source regions as indicated in the upper-right corner of each panel (see Table 1).
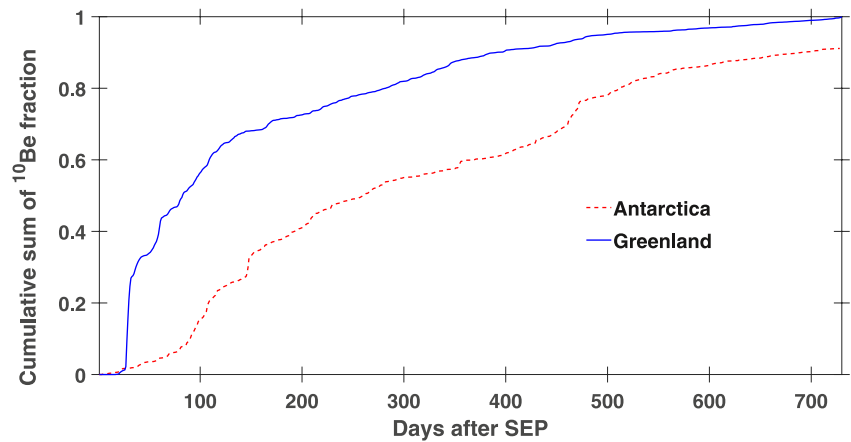
Figure 7. Cumulative zonal mean fraction of the ^{10}Be deposited in the near-ground air at Antarctica (dashed red curve) and Greenland (blue curve), as a function of time following the modeled SEP event on day zero. A major fraction (60–90%) of beryllium is deposited during the first year.

and mountain (e.g., Andes, Himalayas) regions for both scenarios, while the concentrations are much lower in the polar regions, in a qualitative agreement with the previous works (Field et al., 2006; Heikkilä et al., 2009; Zheng et al., 2023). This implies a strong latitudinal gradient in the beryllium concentrations. Since ice-core sites where ^{10}Be is measured are located in polar regions (Greenland and Antarctica) with low beryllium concentrations, precise modeling of its transport and deposition is crucially important for a correct interpretation of the measured concentrations.

4.2. Deposition and Residence Time of ^{10}Be in the Polar Regions

The deposition flux of ^{10}Be is often considered an optimal proxy for cosmic-ray variability (e.g., Heikkilä, Phipps, & Smith, 2013) assuming that all ^{10}Be produced in the atmosphere is deposited at the surface within few years. We estimated, from the model simulation, the residence time of ^{10}Be in the atmosphere depending on the origin region for the SEP scenario with a nearly instant injection of beryllium into the atmosphere. The residence time of ^{10}Be is shown in Figure 6 for the two nearly antipodal locations corresponding to DAS-2 and Vostok sites (see Table 2) following the SEP scenario (0-day is the day of the modeled event) for different source
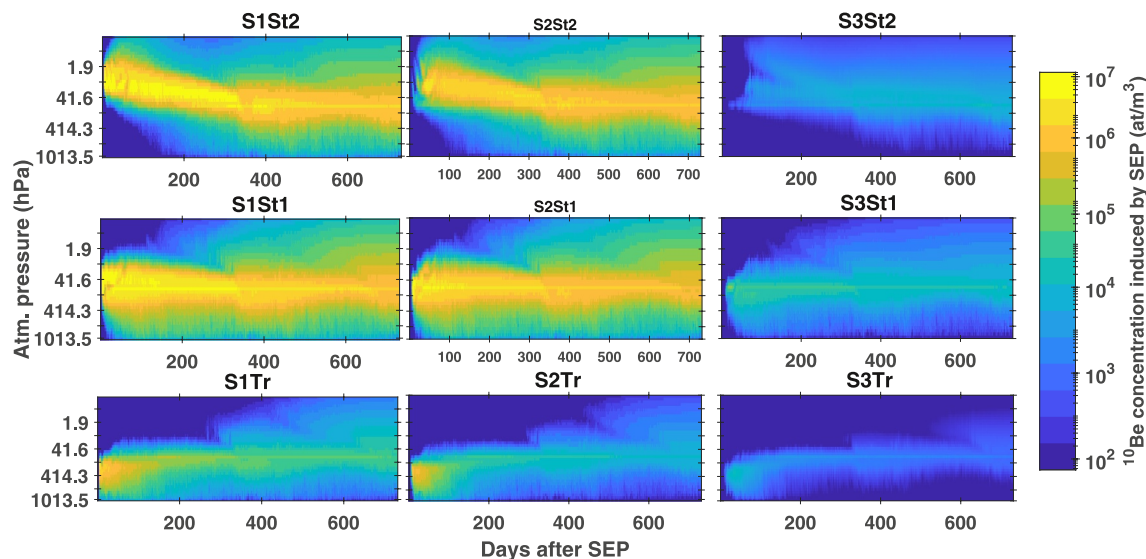

Figure 8. Height (quantified via the atmospheric pressure) distribution of zonal mean ^{10}Be in the Antarctic air as a function of time after the modeled SEP event. Different panels represent different tracers as indicated on the top of each panel (see notations in Table 1).
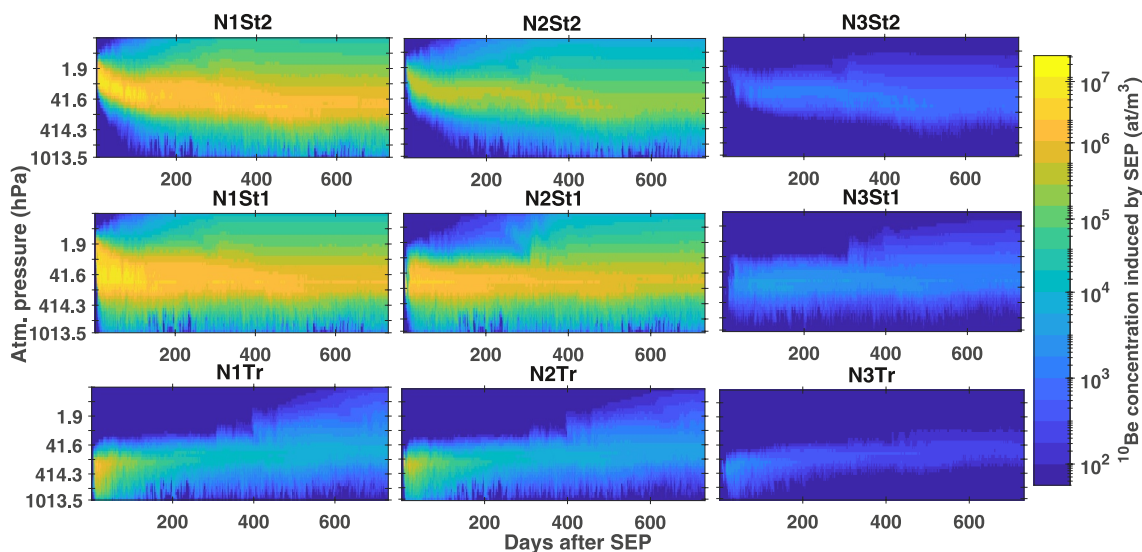
Figure 9. Similar to Figure 8 but for the Greenland.

regions (upper stratosphere and mesosphere are not shown because of their low contributions). According to the model results, there is almost no time delay in the signal corresponding to the tropospheric ^{10}Be production (second and bottom rows of the Figure)—all tropospherically produced beryllium is deposited within a few months. For the beryllium produced in the lower stratosphere (first and third rows in the Figure), the concentration peak is extended for several months, up to almost a year, depending on the season. The residence time for ^{10}Be produced in the upper stratosphere (not shown here) can be more than a year. The beryllium signal delay is affected by the season as being largely defined by the large-scale pattern of the atmospheric circulation and specifically by stratosphere-troposphere exchanges (STEs—Stohl et al., 2003). One can see that there is not much cross-talk between the hemispheres, and the bulk of the SEP-produced beryllium is deposited within 1.5–2 years (more than 85%, see Figure 7). The difference between hemispheres is due to the variation in seasons. In the Northern hemisphere, during the polar winter, the cumulative sum of ^{10}Be fraction is higher because beryllium settles more intensively with precipitation. In contrast, in the Southern hemisphere during summer, precipitation is reduced, resulting in a less intense deposition.
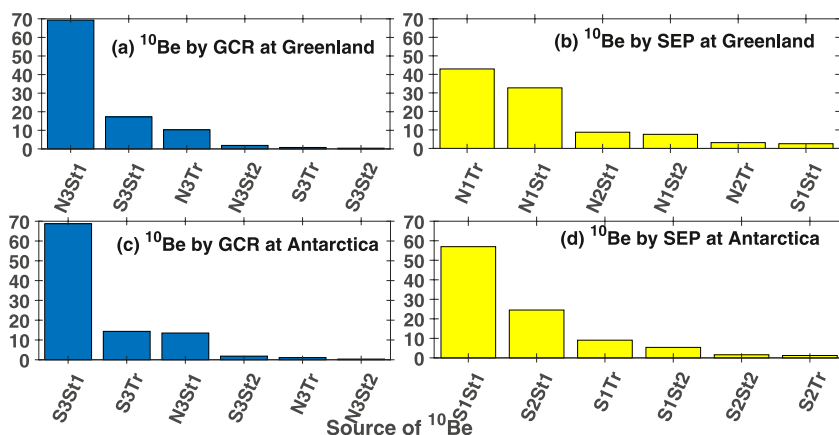
Figure 10. Percentage contribution of the six main source regions of ^{10}Be to the near-ground concentration in polar regions for the GCR (panels a and c) and SEP (panels b and d) scenarios. The notations of the (longitudinally averaged) source regions correspond to Table 1. Panels (a) and (b) correspond to the zonal mean for the North polar region (Greenland), and panels b and d are for the South polar region (Antarctica). In each panel, the six most important regions are shown. The other regions contribute less than 2% altogether.

Table 4
Zonal Mean Partition (Fraction in %) of the Global Production of ^{10}Be by GCR ($Q_{tot} = 1.52 \cdot 10^{17}$ at/sec) Between Different Source Zones (See Notations in Table 1) for the Modern Epoch

Altitude	Latitude zone (i)					
($j \downarrow$)	S1	S2	S3	N3	N2	N1
Tr	3.26	6.81	3.93	4.37	7.73	3.56
St1	9.02	16.58	7.58	8.42	18.06	9.92
St2	0.10	0.14	0.04	0.05	0.17	0.10
Mez	0.01	0.01	0.01	0.01	0.01	0.01

The cumulative zonal-mean beryllium deposition is shown in Figure 7 for the SEP scenario separately for Greenland and Antarctica. The deposition is faster in Greenland, where the SEP event occurs during the local winter, but for both polar regions, a major fraction of SEP-produced beryllium is deposited during the first year, and almost everything within the first 2 years past the event.

Extensions of the modeled concentration-time profiles, shown in Figure 6 for the near-ground air, as a function of height (quantified in the barometric pressure) are shown in Figures 8 and 9 for the Antarctica and Greenland, respectively. As seen, while beryllium is quickly removed from the troposphere, it can stay longer near the tropopause, where it descends from the stratosphere. In addition to the small gravitational settling to the troposphere, sometimes there are STE events as seen, for example, around day 330, viz. during the Austral Spring. During that period, an intrusion of the stratospheric beryllium into the stratosphere is observed as well as the sudden ascend of the tropospheric beryllium into the stratosphere. A similar event is observed ca. day 700, viz. the subsequent Austral Spring. A similar pattern but for the Greenland site (northern hemisphere) is shown in Figure 9.

4.3. Zonal Partition of ^{10}Be Production

Next, we analyzed the ^{10}Be isotope concentrations in polar regions with partitions between different source regions using different tracers as specified in Table 1. The relative percentage contributions from the main source zones to the zonal mean near-ground ^{10}Be in polar regions are shown in Figure 10 for the two regions (Antarctic and Greenland) and the two scenarios (GCR and SEP).

The dominant source of ^{10}Be which eventually resides in Greenland, for the GCR scenario (Figure 10a), is located in the tropical lower stratosphere ($\approx$70% and 17% for the Northern, N3St1, and Southern, S3St1, respectively) followed by Northern tropical troposphere N3Tr ($\approx$10%). Other sources compose only a few per cent altogether. A similar pattern is observed for the Antarctic beryllium in the GCR scenario (panel c), viz. the dominant contribution of about 70% is from the Southern tropical lower stratosphere (S3St1), while the Southern tropical troposphere (S2Tr) and the Northern tropical stratosphere (N3St1) contribute $\approx$ 14% each. Overall, ^{10}Be in polar near-surface air is mostly ($\geq$99%) produced in the entire tropical-zone atmosphere. The importance of the tropical zone is defined by its large area compared to small polar regions. This confirms the earlier results of the full modeling (Heikkilä, Beer, et al., 2013), but disagrees with a simplified approach often used in cosmogenic-isotope studies: globally mixed production or global stratosphere plus polar troposphere (McCracken, 2004).

The situation is different for the SEP scenario (Figure 10, panels b and d) where the isotope is produced mostly in polar regions. The major fraction (about 84%) of ^{10}Be deposited on the Greenland ice caps (panel b) originates from the local polar atmosphere, 43 + 34 + 7% for the troposphere N1Tr, lower N1St1 and upper M1St2 stratospheres, respectively, with $\approx$12% originating from the Northern mid-latitudes. For Antarctica, the polar atmospheric production also dominates (about 75%), with slightly different partitions, viz. 10 +58 + 5% for the troposphere, and lower/upper stratosphere, respectively, and about 25% from the South mid-latitudes. This is in general agreement with previous studies (Heikkilä et al., 2009; Mazaud et al., 1994). Because of the softer energy spectrum of SEPs, they produce beryllium mostly in polar regions with low geomagnetic shielding.

Partition patterns of the global ^{10}Be production between different (longitudinally averaged) source regions are shown in Tables 4 and 5 for the GCR and SEP scenarios for the modern epoch. For the GCR scenario, the production of beryllium is globally spread over the lower stratosphere ($\approx$70%) and troposphere ($\approx$30%), with the upper stratosphere and mesosphere contributing only less than 1% and 0.1%, respectively. Maximum production is predicted in the mid-latitude lower stratosphere (S2St1 and N2St1) as a balance between the geomagnetic shielding (production rate is higher in polar regions) and the geometric factor (the area of the tropical

Table 5
The Same as Table 4, but for ^{10}Be Produced by SEP ($Q_{tot} = 3.99 \cdot 10^{24}$ Atoms)

Altitude	Latitude zone (i)					
($j \downarrow$)	S1	S2	S3	N3	N2	N1
Tr	1.11	0.20	0.0	0.0	0.48	1.43
St1	37.68	4.64	0.0	0.0	13.26	39.03
St2	0.84	0.05	0.0	0.0	0.25	0.75
Mez	0.10	0.01	0.0	0.0	0.02	0.01

Table 6

Transport Coefficients ($Z_{i,j}$) for ^{10}Be Between Different Source Zones (See Notations in Table 1) and the Time Parameter τ Using for Parametrization (Equation 4) for the GCR Scenario in Case of 18 Tracers

Region	V, m^3	τ, sec		Tr	St	St2
					$Z_{i,j}$	
Antarctica	7.56E+14	13,829	S1	7.88E−02	7.24E−03	5.07E−03
			S2	1.15E−02	5.06E−03	4.74E−03
			S3	4.57E−04	2.03E−03	3.77E−03
			N3	3.27E−05	5.64E−04	1.74E−03
			N2	5.30E−06	2.86E−04	8.21E−04
			N1	2.50E−06	2.46E−04	6.67E−04
Greenland	1.28E+14	16,575	S1	2.12E−06	7.41E−05	2.05E−04
			S2	1.17E−06	9.19E−05	2.67E−04
			S3	6.61E−06	1.58E−04	4.60E−04
			N3	7.56E−05	5.05E−04	8.82E−04
			N2	1.71E−03	1.15E−03	1.06E−03
			N1	1.03E−02	1.53E−03	1.08E−03

zone is largest). The pattern is different for the SEP scenario (Table 5), where the dominant production occurs in the polar lower stratosphere ($\approx$77% in S1St1+N1St1 regions) due to the strong geomagnetic cutoff applied to the soft SEP energy spectrum. Mid-latitude lower stratosphere contributes about 18% to the total production of ^{10}Be, while the polar troposphere only about 5%. Almost no beryllium is produced in the tropical zone for the SEP scenario. We note that the exact percentiles depend on the geomagnetic shielding, and the values presented in Tables 4 and 5 correspond to the modern era and should not be used for other geomagnetic epochs.

4.4. Parameterization

After making the full simulations of the 96 selected ^{10}Be tracers (Table 1), we next parameterized the surface concentration of the beryllium isotope at a given location in a way that it can be approximately estimated only from the production pattern without direct modeling of the transport and concentration, viz. similar to the parameterization introduced by Heikkilä, Phipps, and Smith (2013).

The surface concentration of ^{10}Be in a given location (specified by an index n), further denoted as C_n, is defined as a sum of the concentrations from different sources as denoted by indices i, j, and k (latitude, altitude, and longitude respectively—see Table 1):

$$C_n = \sum_{i,j,k} C_{i,j,k,n} \tag{3}$$

the near-ground concentration of ^{10}Be in location n from the source region i, j, k can be defined, in the quasi-equilibrium case, as

$$C_{i,j,k,n} = \frac{Q_{i,j,k} \cdot Z_{i,j,k,n} \cdot \tau_n}{V_n}, \tag{4}$$

where $Q_{i,j,k}$ is the isotope's annual mean production rate in the region (i, j, k) in at/sec (for the SEP scenario, it is defined as the total number of ^{10}Be atoms produced by SEPs divided by the number of seconds in 1 year, $3.156 \cdot 10^7$ s); $Z_{i,j,k,n}$ is a transport coefficient quantifying the fraction of beryllium produced in the source region (i, j, k) to appear at location n (can be found in Golubenko (2023) for both GCR and SEP scenarios); τ_n is the time (in seconds) characteristic of deposition of beryllium from the near-ground air; V_n is a model cell volume in m^3 for the given location (see Golubenko, 2023, or Table 7). The value of τ_n is the only free parameter in the approach which is defined in an ad-hoc manner separately for the Antarctic and Greenland regions so that the parameterized mean ^{10}Be concentration in the selected region is equal to that computed by the full model. Thus defined values of τ comprise about 4 hours for the GCR scenario (see Table 6) and about six-seven hours for the SEP scenario (see Table 7). In the case of Scenario 1, the values of τ are symmetric between the two hemispheres, whereas, for Scenario 2, they differ by more than an hour between the hemispheres, as the season when the solar event occurred plays a crucial role here.

The values of the source-region production rates $Q_{i,j,k}$ need to be computed independently, using the isotope's production model (e.g., Poluianov et al., 2016), or for the modern epoch, estimated as

Table 7

The Same as Table 6 but for the SEP Scenario

| Region	V, m^3	τ, sec		Tr	St	St2
					$Z_{i,j}$	
Antarctica	7.56E+14	27,000	S1	2.24E−02	6.72E−03	5.75E−03
			S2	1.35E−02	7.37E−03	5.45E−03
			S3	8.96E−04	4.93E−03	4.51E−03
			N3	4.37E−06	2.20E−04	2.07E−04
			N2	6.29E−06	2.05E−04	1.91E−04
			N1	5.00E−06	1.59E−04	1.86E−04
Greenland	1.28E+14	20,001	S1	9.09E−06	4.66E−05	4.50E−05
			S2	1.54E−06	4.42E−05	5.38E−05
			S3	1.99E−06	5.38E−05	5.26E−05
			N3	2.37E−04	5.66E−04	1.12E−03
			N2	4.27E−03	1.11E−03	1.17E−03
			N1	9.15E−03	1.22E−03	1.20E−03
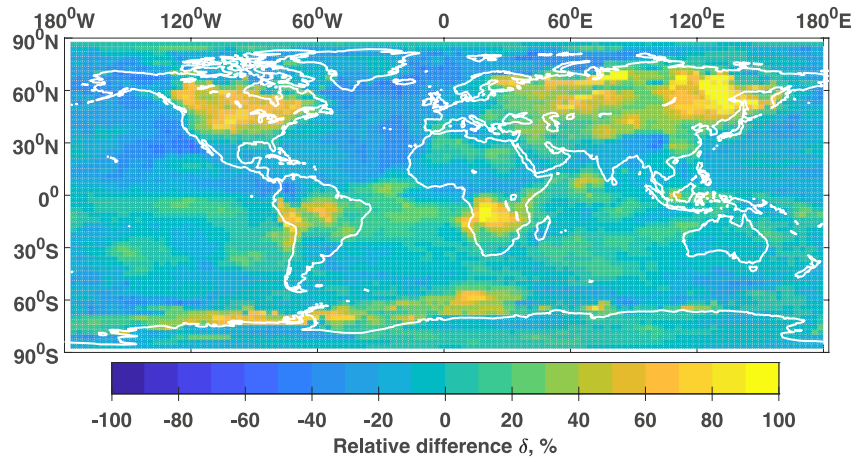
Figure 11. Geographical distribution of the mean relative difference $\delta = (P - M)/M$ between the parameterized (P) and full-model (M) near-surface air concentrations of ^{10}Be for the period 1980–1990.

$$Q_{i,j,k} = Q_{\text{tot}} \cdot S_{i,j,k}, \tag{5}$$

where $S_{i,j,k}$ is the partition of the total isotope's production rate Q_{tot} between the source regions (for modern epoch, it can be found in Tables 4 and 5 for the GCR and SEP scenarios, respectively).

As seen in Tables 4 and 5, the contribution of beryllium produced in the mesosphere to the polar near-ground concentration is less than 1%, so we can neglect it in the parameterization results. To simplify the procedure further, we used zonal means, resulting in the parameterization based on only 18 tracers. The above approach was used to define the parameters in Tables 6 and 7.

Figure 11 shows the ratio between the ^{10}Be surface concentrations computed using the above parametrization (Formulas 3–5) and the full model. The agreement between the parameterization and the full model is good (within 20%) over the major part of the globe except for several regions with a larger (up to a factor of two) difference which are related to continental locations with high precipitation levels. Since measurements of ^{10}Be are mostly performed in polar ice cores, we report that the two approaches agree within 15% in polar regions: Antarctica and Greenland.

Figure 12 depicts an example of the parametrization results averaged over Greenland and Antarctica regions for the GCR scenario for the period 1980–1990. The agreement is good, being within 1% for the overall level and 5
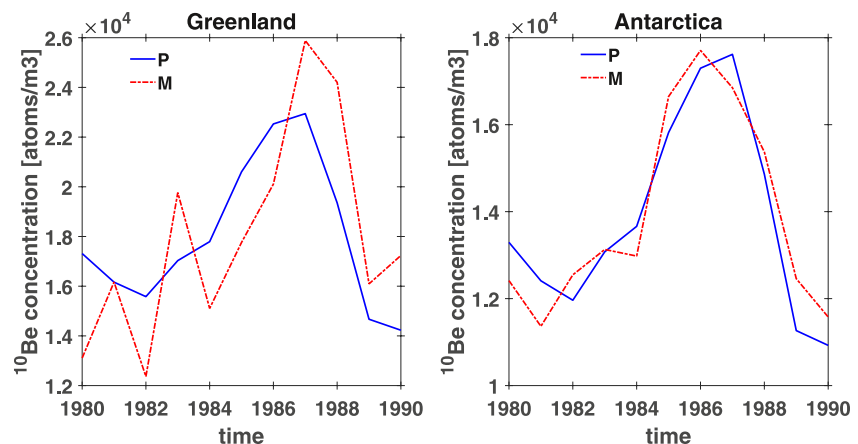

Figure 12. Averaged near-ground concentrations of ^{10}Be over Greenland and Antarctica as computed by the full model (red dashed M-curve) and the parametrization (solid blue P-curve) over one solar cycle 1980–1990.

(15)% for the interannual variability in the Antarctic (Greenland) regions, respectively. Interestingly, while ^{10}Be data at individual sites are dominated by the regional climate signal at the inter-annual scale and do not depict a distinguishable solar cycle (cf., 3), the zonal mean variability clearly follows the solar cycle. An example of the use of the proposed parameterization to calculate the ^{10}Be near-ground concentration in the Antarctica region is shown in Appendix A.

5. Conclusions

Here we present a new full model of production and transport of the cosmogenic isotope ^{10}Be in the Earth's atmosphere using the CCM SOCOL-AERv2-BE for two distinct scenarios, viz. the continuous production by omnipresent and slightly variable galactic cosmic rats (GCR scenario) and a short impulsive production by SEP scenario. The full model has been directly validated by measurements of ^{10}Be in ice cores and near-ground air in antipodal polar locations—in Antarctica and Greenland for the period 1980–2007. The model correctly reproduces the overall in-air concentration and the solar-cycle variability (or the lack of such) of beryllium in most locations except for the near-shore Eastern-Greenland site DAS-2 but is not precise at the (inter)annual time scale where the local climatic noise dominate the signal. The discrepancy is likely caused by a too-rough grid size of the model which cannot capture the complex orography of the high-altitude polar locations. It is demonstrated that the dominant region of ^{10}Be production is the tropical stratosphere for the GCR scenario, while for the SEP scenario, it is the polar stratosphere. The residence time of ^{10}Be in the atmosphere varies from 1 to 2.5 years depending on the source region, but on average, >90% of the produced beryllium is deposited within 2 years.

The results of the full modeling including 96 ^{10}Be tracers including a code to calculate ^{10}Be concentrations using pre-computed transport coefficients are available in Golubenko (2023). In addition, here we also provide a simple-to-use parameterization for the results of the full model so that the near-ground-air concentration of ^{10}Be in polar regions can be easily calculated using tabulated transport coefficients, without full modeling, for any given isotope production rate partitioned between 18 source regions: three altitude zones (troposphere, lower and upper stratosphere) and six latitude zones (tropical, mid-latitude and polar zones, separately for each hemisphere). The transport coefficients are tabulated separately for the GCR and SEP scenarios. The accuracy of the parameterization is within 20% of the full model.

In conclusion, the presented and validated full model of the atmospheric production and transport of ^{10}Be provides a new precise tool to study cosmic-ray variability using cosmogenic tracers. The results of the model will be used for a refined analysis of the cosmogenic data for the study of solar activity and climate variability in the past.

Appendix A: Example of the Calculation of ^{10}Be Concentrations in Near-Ground Air at Antarctica for the GCR Scenario for 1980

To calculate the concentration of ^{10}Be in near-ground air, one needs first to know the global production rate of the isotope, which can be computed, for example, using the CRAC model (Poluianov et al., 2016), for a given geomagnetic rigidity cutoff (see, e.g., Kovaltsov & Usoskin, 2007).

As an example, let us consider the GCR-produced ^{10}Be for the year 1980. The global production of ^{10}Be for 1980 is estimated, using the model by Poluianov et al. (2016) as $Q_{\text{tot}} = 1.4159 \cdot 10^{+17}$ at/sec. Then, the near-ground-air concentration of ^{10}Be the Southern polar region (Antarctica) can be computed in the following steps described below.

Step I: Using Q_{tot} above and values of $S_{i,j}$ from Table 4, and applying Formula 5, one can find the ^{10}Be production rates at different source regions, $Q_{i,j}$. The production in the mesosphere is neglected and the zonal mean production rates are used. As a result, we have the production rates in 18 sources:
The $S_{1,1}$ value for the region (1, 1), viz. the Southern polar troposphere S1Tr, is 3.26% (see Table 4), and thus the production rate in this region is defined as

$$Q_{1,1} = Q_{\text{tot}} \times (Q_{1,1}/100) = 1.4159 \cdot 10^{17} \times 0.0326 = 4.61 \cdot 10^{15} \text{ at/sec.}$$

Similarly

$$Q_{1,2} = Q_{\text{tot}} \times (Q_{1,2}/100) = 1.4159 \cdot 10^{17} \times 0.0902 = 1.27 \cdot 10^{16} \text{ at/sec.}$$

...

$$Q_{3,3} = Q_{\text{tot}} \times (Q_{3,3}/100) = 5.66 \cdot 10^{13} \text{ at/sec.}$$

Production rates for the sources in the Northern Hemisphere, $Q_{4,1}$—$Q_{6,3}$ can be calculated in the same way.

Step II: Using Formula 4, one can calculate the near-ground concentration of ^{10}Be in the Antarctica region from each source region, taking the values of the cell volume (V), partition ($Z_{i,j}$), and the time parameter (τ) from Table 6:

$C_{1,1} = (Q_{1,1} \times Z_{1,1} \times \tau_1)/V_1 = 4.61 \cdot 10^{15} \times 7.88 \cdot 10^{-2} \times 13{,}829/7.56 \cdot 10^{14} = 6.64 \cdot 10^3$ at/m^3.

$\quad C_{1,2} = (Q_{1,2} \times Z_{1,2} \times \tau_1)/V_1 = 1.27 \cdot 10^{16} \times 7.24 \cdot 10^{-3} \times 13{,}829/7.56 \cdot 10^{14} = 1.68 \cdot 10^3$ at/m^3.

…

Step III: Finally, using Formula 3, one can calculate the near-ground concentration of ^{10}Be in the Antarctica region as:

$\quad C = C_{1,1} + C_{1,2} + C_{1,3} + C_{2,1} + \cdots + C_{6,3} = 1.33 \cdot 10^4$ at/m^{-3},

which can be found as the leftmost blue point in Figure 12b.

A1. Example of the Calculation of ^{10}Be Concentration in Near-Ground Air at Antarctica for the SEP Scenario

The ^{10}Be concentration in near-ground air for the SEP scenario can be calculated in the same way as for the GCR scenario above, with the only difference being the total global production Q_{tot}. The total amount of ^{10}Be produced in the atmosphere within the SEP scenario was estimated as $3.996 \cdot 10^{24}$. When uniformly spread over the entire year ($3.1536 \cdot 10^7$ s), this leads to the global annual production rate $Q = 1.261 \cdot 10^{17}$ at/sec. Applying the same steps I–III described above, one can get the near-ground-air concentration of ^{10}Be in the Antarctica region as $1.49 \cdot 10^4$ at/m^3. We note that this assumes that all the SEP-produced ^{10}Be atoms are settled down within one year past the event neglecting the time profile shown in Figure 7.

Data Availability Statement

CCM SOCOL-AERv2-BE used for paper is preserved at link Golubenko, Rozanov, Sukhodolov, and Usoskin (2021). Matlab code and all files for parameterization are available at Golubenko (2023).

References

Adolphi, F., Herbst, K., Nilsson, A., & Panovska, S. (2023). On the polar bias in ice core ^{10}be data. *Journal of Geophysical Research: Atmospheres*, *128*(4), e2022JD038203. https://doi.org/10.1029/2022jd038203

Agostinelli, S., Allison, J., Amako, K., Apostolakis, J., Araujo, H., Arce, P., et al. (2003). GEANT4 – A simulation toolkit. *Nuclear Instruments and Methods in Physics Research A*, *506*(3), 250–303. https://doi.org/10.1016/S0168-9002(03)01368-8

Arnold, M., Merchel, S., Bourlès, D. L., Braucher, R., Benedetti, L., Finkel, R. C., et al. (2010). The French accelerator mass spectrometry facility aster: Improved performance and developments. *Nuclear Instruments and Methods in Physics Research Section B: Beam Interactions with Materials and Atoms*, *268*(11), 1954–1959. https://doi.org/10.1016/j.nimb.2010.02.107

Bard, E., Raisbeck, G., Yiou, F., & Jouzel, J. (1997). Solar modulation of cosmogenic nuclide production over the last millennium: Comparison between ^{14}C and ^{10}Be records. *Earth and Planetary Science Letters*, *150*(3–4), 453–462. https://doi.org/10.1016/S0012-821X(97)00082-4

Baroni, M., Bard, E., Petit, J.-R., Magand, O., & Bourlès, D. (2011). Volcanic and solar activity, and atmospheric circulation influences on cosmogenic ^{10}Be fallout at Vostok and Concordia (Antarctica) over the last 60 years. *Geochimica et Cosmochimica Acta*, *75*(22), 7132–7145. https://doi.org/10.1016/j.gca.2011.09.002

Baroni, M., Bard, E., Petit, J.-R., & Viseur, S. (2019). Persistent draining of the stratospheric ^{10}Be reservoir after the Samalas Volcanic eruption (1257 CE). *Journal of Geophysical Research: Atmospheres*, *124*(13), 7082–7097. https://doi.org/10.1029/2018JD029823

Beer, J., McCracken, K., & von Steiger, R. (2012). *Cosmogenic radionuclides: Theory and applications in the terrestrial and space environments*. Springer.

Butchart, N. (2014). The Brewer-Dobson circulation. *Reviews of Geophysics*, *52*(2), 157–184. https://doi.org/10.1002/2013RG000448

Caballero-Lopez, R. A., Moraal, H., McCracken, K. G., & McDonald, F. B. (2004). The heliospheric magnetic field from 850 to 2000 AD inferred from ^{10}Be records. *Journal of Geophysical Research*, *109*(A18), A12102. https://doi.org/10.1029/2004JA010633

Cliver, E., Schrijver, C., Shibata, K., & Usoskin, I. (2022). Extreme solar events. *Living Reviews in Solar Physics*, *19*(2), 2. https://doi.org/10.1007/s41116-022-00033-8

Cooke, D., Humble, J., Shea, M., Smart, D., Lund, N., Rasmussen, I., et al. (1991). On cosmic-ray cut-off terminology. *Nuovo Cimento della Società Italiana di Fisica - C: Geophysics and Space Physics*, *14*(3), 213–234. https://doi.org/10.1007/bf02509357

Dee, D. P., Uppala, S. M., Simmons, A. J., Berrisford, P., Poli, P., Kobayashi, S., et al. (2011). The Era-Interim reanalysis: Configuration and performance of the data assimilation system. *Quarterly Journal of the Royal Meteorological Society*, *137*(656), 553–597. https://doi.org/10.1002/qj.828

Delaygue, G., & Bard, E. (2011). An Antarctic view of Beryllium-10 and solar activity for the past millennium. *Climate Dynamics*, *36*(11–12), 2201–2218. https://doi.org/10.1007/s00382-010-0795-1

Delaygue, G., Bekki, S., & Bard, E. (2015). Modelling the stratospheric budget of beryllium isotopes. *Tellus Series B Chemical and Physical Meteorology*, *67*(1), 28582. https://doi.org/10.3402/tellusb.v67.28582

Dibb, J. E., Meeker, L. D., Finkel, R. C., Southon, J. R., Caffee, M. W., & Barrie, L. A. (1994). Estimation of stratospheric input to the arctic troposphere: ^{7}Be and ^{10}Be in aerosols at alert, Canada. *Journal of Geophysical Research*, *99*(D6), 12855–12864. https://doi.org/10.1029/94JD00742

Egorova, T., Rozanov, E., Zubov, V., & Karol, I. (2003). Model for investigating ozone trends (MEZON). *Izvestiya - Atmospheric and Oceanic Physics*, *39*, 277–292.

Elsässer, C., Wagenbach, D., Weller, R., Auer, M., Wallner, A., & Christl, M. (2011). Continuous 25-yr aerosol records at coastal Antarctica. *Tellus B: Chemical and Physical Meteorology*, *63*(5), 920–934. https://doi.org/10.1111/j.1600-0889.2011.00543.x

Feinberg, A., Sukhodolov, T., Luo, B.-P., Rozanov, E., Winkel, L. E., Peter, T., & Stenke, A. (2019). Improved tropospheric and stratospheric sulfur cycle in the aerosol-chemistry-climate model SOCOL-AERv2. *Geoscientific Model Development*, *12*(9), 3863–3887. https://doi.org/10.5194/gmd-12-3863-2019

Field, C., Schmidt, G., Koch, D., & Salyk, C. (2006). Modeling production and climate-related impacts on ^{10}Be concentration in ice cores. *Journal of Geophysical Research*, *111*(D15), D15107. https://doi.org/10.1029/2005jd006410

Golubenko, K. (2023). Matlab tools for parametrization of 10be concentration induced by gcr/sep using ccm socol-aerv2-be simulation. *Zenodo*. https://doi.org/10.5281/zenodo.10592405

Golubenko, K., Rozanov, E., Kovaltsov, G., Leppänen, A.-P., Sukhodolov, T., & Usoskin, I. (2021a). Chemistry-climate model socol-aerv2-bev1 with the cosmogenic beryllium-7 isotope cycle. *Geoscientific Model Development Discussions*, *2021*, 1–24. https://doi.org/10.5194/gmd-2021-56

Golubenko, K., Rozanov, E., Kovaltsov, G., & Usoskin, I. (2022). Zonal mean distribution of cosmogenic isotope (7be, 10be, 14c, and 36cl) production in stratosphere and troposphere. *Journal of Geophysical Research: Atmospheres*, *127*(16), e2022JD036726. https://doi.org/10.1029/2022JD036726

Golubenko, K., Rozanov, E., Sukhodolov, T., & Usoskin, I. (2021b). CCM SOCOL-AERv2-BEv1. [Software]. *Zenodo*. https://doi.org/10.5281/zenodo.5006356

Grinsted, A., Moore, J. C., & Jevrejeva, S. (2004). Application of the cross wavelet transform and wavelet coherence to geophysical time series. *Nonlinear Processes in Geophysics*, *11*(5/6), 561–566. https://doi.org/10.5194/npg-11-561-2004

Heikkilä, U., Beer, J., Abreu, J. A., & Steinhilber, F. (2013a). On the atmospheric transport and deposition of the cosmogenic Radionuclides (^{10}Be): A review. *Space Science Reviews*, *176*(1–4), 321–332. https://doi.org/10.1007/s11214-011-9838-0

Heikkilä, U., Beer, J., & Feichter, J. (2009). Meridional transport and deposition of atmospheric ^{10}Be. *Atmospheric Chemistry and Physics*, *9*(2), 515–527. https://doi.org/10.5194/acp-9-515-2009

Heikkilä, U., Phipps, S. J., & Smith, A. M. (2013b). ^{10}Be in late deglacial climate simulated by ECHAM5-HAM - Part 1: Climatological influences on ^{10}Be deposition. *Climate of the Past*, *9*(6), 2641–2649. https://doi.org/10.5194/cp-9-2641-2013

Herbst, K., Kopp, A., & Heber, B. (2013). Influence of the terrestrial magnetic field geometry on the cutoff rigidity of cosmic ray particles. *Annales Geophysicae*, *31*(10), 1637–1643. https://doi.org/10.5194/angeo-31-1637-2013

Hersbach, H., Bell, B., Berrisford, P., Hirahara, S., Horányi, A., Muñoz-Sabater, J., et al. (2020). The Era5 global reanalysis. *Quarterly Journal of the Royal Meteorological Society*, *146*(730), 1999–2049. https://doi.org/10.1002/qj.3803

Hommel, R., Timmreck, C., & Graf, H. F. (2011). The global middle-atmosphere aerosol model MAECHAM5-SAM2: Comparison with satellite and in-situ observations. *Geoscientific Model Development*, *4*(3), 809–834. https://doi.org/10.5194/gmd-4-809-2011

Koldobskiy, S. A., Raukunen, O., Vainio, R., Kovaltsov, G., & Usoskin, I. (2021). New reconstruction of event-integrated spectra (spectral fluences) for major solar energetic particle events. *Astronomy and Astrophysics*, *647*, A132. https://doi.org/10.1051/0004-6361/202040058

Kovaltsov, G., & Usoskin, I. (2010). A new 3D numerical model of cosmogenic nuclide ^{10}Be production in the atmosphere. *Earth and Planetary Science Letters*, *291*(1–4), 182–188. https://doi.org/10.1016/j.epsl.2010.01.011

Kovaltsov, G. A., & Usoskin, I. G. (2007). Regional cosmic ray induced ionization and geomagnetic field changes. *Advances in Geosciences*, *13*, 31–35. https://doi.org/10.5194/adgeo-13-31-2007

Lal, D., & Suess, H. (1968). The radioactivity of the atmosphere and hydrosphere. *Annual Review of Nuclear Science*, *18*(1), 407–434. https://doi.org/10.1146/annurev.ns.18.120168.002203

Legrand, M., Preunkert, S., Weller, R., Zipf, L., Elsässer, C., Merchel, S., et al. (2017a). Year-round record of bulk and size-segregated aerosol composition in Central Antarctica (concordia site) – Part 2: Biogenic sulfur (sulfate and methanesulfonate) aerosol. *Atmospheric Chemistry and Physics*, *17*(22), 14055–14073. https://doi.org/10.5194/acp-17-14055-2017

Legrand, M., Preunkert, S., Wolff, E., Weller, R., Jourdain, B., & Wagenbach, D. (2017b). Year-round records of bulk and size-segregated aerosol composition in central Antarctica (concordia site) – Part 1: Fractionation of sea-salt particles. *Atmospheric Chemistry and Physics*, *17*(22), 14039–14054. https://doi.org/10.5194/acp-17-14039-2017

Leppänen, A.-P., Pacini, A. A., Usoskin, I. G., Aldahan, A., Echer, E., Evangelista, H., et al. (2010). Cosmogenic ^{7}Be in air: A complex mixture of production and transport. *Journal of Atmospheric and Solar-Terrestrial Physics*, *72*(13), 1036–1043. https://doi.org/10.1016/j.jastp.2010.06.006

Masarik, J., & Beer, J. (1999). Simulation of particle fluxes and cosmogenic nuclide production in the Earth's atmosphere. *Journal of Geophysical Research*, *104*(D10), 12099–12111. https://doi.org/10.1029/1998jd200091

Mazaud, A., Laj, C., & Bender, M. (1994). A geomagnetic chronology for Antarctic ice accumulation. *Geophysical Research Letters*, *21*(5), 337–340. https://doi.org/10.1029/93GL02789

McCracken, K. (2004). Geomagnetic and atmospheric effects upon the cosmogenic ^{10}Be observed in polar ice. *Journal of Geophysical Research*, *109*(A18). https://doi.org/10.1029/2003JA010060

Miyake, F., Nagaya, K., Masuda, K., & Nakamura, T. (2012). A signature of cosmic-ray increase in ad 774-775 from tree rings in Japan. *Nature*, *486*(7402), 240–242. https://doi.org/10.1038/nature11123

Miyake, F., Usoskin, I., & Poluianov, S. (Eds.) (2019)., *Extreme solar particle storms: The hostile sun*. IOP Publishing. https://doi.org/10.1088/2514-3433/ab404a

Nevalainen, J., Usoskin, I. G., & Mishev, A. (2013). Eccentric dipole approximation of the geomagnetic field: Application to cosmic ray computations. *Advances in Space Research*, *52*(1), 22–29. https://doi.org/10.1016/j.asr.2013.02.020

Pedro, J. B., McConnell, J. R., van Ommen, T. D., Fink, D., Curran, M. A. J., Smith, A. M., et al. (2012). Solar and climate influences on ice core ^{10}Be records from Antarctica and Greenland during the neutron monitor era. *Earth and Planetary Science Letters*, *355*, 174–186. https://doi.org/10.1016/j.epsl.2012.08.038

Poluianov, S., Kovaltsov, G. A., Mishev, A. L., & Usoskin, I. G. (2016). Production of cosmogenic isotopes ^{7}Be, ^{10}Be, ^{14}C, ^{22}Na, and ^{36}Cl in the atmosphere: Altitudinal profiles of yield functions. *Journal of Geophysical Research: Atmospheres*, *121*(13), 8125–8136. https://doi.org/10.1002/2016JD025034

Simon, K., Pedro, J., Smith, A., Child, D., & Fink, D. (2013). Reprocessing of 10b-contaminated 10be ams targets. *Nuclear Instruments and Methods in Physics Research Section B: Beam Interactions with Materials and Atoms*, *294*, 208–213. https://doi.org/10.1016/j.nimb.2012.07.013

Spiegl, T. C., Yoden, S., Langematz, U., Sato, T., Chhin, R., Noda, S., et al. (2022). Modeling the transport and deposition of ^{10}Be produced by the strongest solar proton event during the Holocene. *Journal of Geophysical Research: Atmospheres*, *127*(13), e2021JD035658. https://doi.org/10.1029/2021JD035658

Stenke, A., Schraner, M., Rozanov, E., Egorova, T., Luo, B., & Peter, T. (2013). The SOCOL version 3.0 chemistry-climate model: Description, evaluation, and implications from an advanced transport algorithm. *Geoscientific Model Development*, *6*(5), 1407–1427. https://doi.org/10.5194/gmd-6-1407-2013

Stohl, A., Bonasoni, P., Cristofanelli, P., Collins, W., Feichter, J., Frank, A., et al. (2003). Stratosphere-troposphere exchange: A review, and what we have learned from staccato. *Journal of Geophysical Research*, *108*(D12). https://doi.org/10.1029/2002JD002490

Sukhodolov, T., Usoskin, I., Rozanov, E., Asvestari, E., Ball, W., Curran, M., et al. (2017). Atmospheric impacts of the strongest known solar particle storm of 775 AD. *Scientific Reports*, *7*(1), 45257. https://doi.org/10.1038/srep45257

Thébault, E., Finlay, C. C., Beggan, C. D., Alken, P., Aubert, J., Barrois, O., et al. (2015). International geomagnetic reference field: The 12th generation. *Earth Planets and Space*, *67*(1), 79. https://doi.org/10.1186/s40623-015-0228-9

Usoskin, I. G. (2023). A history of solar activity over millennia. *Living Reviews in Solar Physics*, *20*(1), 2. https://doi.org/10.1007/s41116-023-00036-z

Usoskin, I. G., Alanko-Huotari, K., Kovaltsov, G. A., & Mursula, K. (2005). Heliospheric modulation of cosmic rays: Monthly reconstruction for 1951–2004. *Journal of Geophysical Research*, *110*(A12), A12108. https://doi.org/10.1029/2005JA011250

Usoskin, I. G., Bazilevskaya, G. A., & Kovaltsov, G. A. (2011). Solar modulation parameter for cosmic rays since 1936 reconstructed from ground-based neutron monitors and ionization chambers. *Journal of Geophysical Research*, *116*(A2), A02104. https://doi.org/10.1029/2010JA016105

Usoskin, I. G., Field, C. V., Schmidt, G. A., Leppänen, A.-P., Aldahan, A., Kovaltsov, G. A., et al. (2009a). Short-term production and synoptic influences on atmospheric ^{7}Be concentrations. *Journal of Geophysical Research*, *114*(D13), D06108. https://doi.org/10.1029/2008JD011333

Usoskin, I. G., Gallet, Y., Lopes, F., Kovaltsov, G. A., & Hulot, G. (2016). Solar activity during the holocene: The Hallstatt cycle and its consequence for grand minima and maxim. *Astronomy and Astrophysics*, *587*, A150. https://doi.org/10.1051/0004-6361/201527295

Usoskin, I. G., Gil, A., Kovaltsov, G. A., Mishev, A. L., & Mikhailov, V. V. (2017). Heliospheric modulation of cosmic rays during the neutron monitor era: Calibration using PAMELA data for 2006-2010. *Journal of Geophysical Research: Space Physics*, *122*(4), 3875–3887. https://doi.org/10.1002/2016JA023819

Usoskin, I. G., Horiuchi, K., Solanki, S., Kovaltsov, G. A., & Bard, E. (2009b). On the common solar signal in different cosmogenic isotope data sets. *Journal of Geophysical Research*, *114*(A13), A03112. https://doi.org/10.1029/2008JA013888

Usoskin, I. G., Koldobskiy, S., Kovaltsov, G., Rozanov, E., Sukhodolov, T., Mishev, A., & Mironova, I. (2020). Revisited reference solar proton event of 23 February 1956: Assessment of the cosmogenic-isotope method sensitivity to extreme solar events. *Journal of Geophysical Research: Space Physics*, *125*(6), e27921. https://doi.org/10.1029/2020JA027921

Usoskin, I. G., Korte, M., & Kovaltsov, G. A. (2008). Role of centennial geomagnetic changes in local atmospheric ionization. *Geophysical Research Letters*, *35*(5), L05811. https://doi.org/10.1029/2007GL033040

Usoskin, I. G., & Kovaltsov, G. A. (2008). Production of cosmogenic ^{7}Be isotope in the atmosphere: Full 3D modelling. *Journal of Geophysical Research*, *113*(D12), D12107. https://doi.org/10.1029/2007JD009725

Usoskin, I. G., Kromer, B., Ludlow, F., Beer, J., Friedrich, M., Kovaltsov, G. A., et al. (2013). The AD775 cosmic event revisited: The Sun is to blame. *Astronomy and Astrophysics*, *552*, L3. https://doi.org/10.1051/0004-6361/201321080

Väisänen, P., Usoskin, I., Kähkönen, R., Koldobskiy, S., & Mursula, K. (2023). Revised reconstruction of the heliospheric modulation potential for 1964-2022. *Journal of Geophysical Research: Space Physics*, *128*(4), e2023JA031352. https://doi.org/10.1029/2023JA031352

van Ommen, T., & Morgan, V. (2010). Snowfall increase in coastal East Antarctica linked with southwest Western Australian drought. *Nature Geoscience*, *3*(4), 267–272. https://doi.org/10.1038/ngeo761

Vos, E. E., & Potgieter, M. S. (2015). New modeling of galactic proton modulation during the minimum of solar cycle 23/24. *The Astrophysical Journal*, *815*(2), 119. https://doi.org/10.1088/0004-637X/815/2/119

Wu, C. J., Usoskin, I. G., Krivova, N., Kovaltsov, G. A., Baroni, M., Bard, E., & Solanki, S. K. (2018). Solar activity over nine millennia: A consistent multi-proxy reconstruction. *Astronomy and Astrophysics*, *615*, A93. https://doi.org/10.1051/0004-6361/201731892

Zheng, M., Adolphi, F., Ferrachat, S., Mekhaldi, F., Lu, Z., Nilsson, A., & Lohmann, U. (2024). Modeling atmospheric transport of cosmogenic radionuclide ^{10}Be using geos-chem 14.1.1 and echam6.3-ham2.3: Implications for solar and geomagnetic reconstructions. *Geophysical Research Letters*, *51*(2), e2023GL106642. https://doi.org/10.1029/2023GL106642

Zheng, M., Adolphi, F., Sjolte, J., Aldahan, A., Possnert, G., Wu, M., et al. (2020). Solar and climate signals revealed by seasonal ^{10}Be data from the neem ice core project for the neutron monitor period. *Earth and Planetary Science Letters*, *541*, 116273. https://doi.org/10.1016/j.epsl.2020.116273

Zheng, M., Liu, H., Adolphi, F., Muscheler, R., Lu, Z., Wu, M., & Prisle, N. L. (2023). Simulations of ^{7}be and ^{10}be with the geos-chem global model v14.0.2 using state-of-the-art production rates. *Geoscientific Model Development*, *16*(23), 7037–7057. https://doi.org/10.5194/gmd-16-7037-2023